Science and Technology of Advanced Materials

ISSN: 1468-6996 (Print) 1878-5514 (Online) Journal homepage: https://www.tandfonline.com/loi/tsta20

New intelligent multifunctional SiO_2/VO_2 composite films with enhanced infrared light regulation performance, solar modulation capability, and superhydrophobicity

Chao Wang, Li Zhao, Zihui Liang, Binghai Dong, Li Wan & Shimin Wang

To cite this article: Chao Wang, Li Zhao, Zihui Liang, Binghai Dong, Li Wan & Shimin Wang (2017) New intelligent multifunctional SiO_2/VO_2 composite films with enhanced infrared light regulation performance, solar modulation capability, and superhydrophobicity, Science and Technology of Advanced Materials, 18:1, 563-573, DOI: 10.1080/14686996.2017.1360752

To link to this article: https://doi.org/10.1080/14686996.2017.1360752

Published online: 22 Aug 2017.

SCIENCE AND TECHNOLOGY OF ADVANCED MATERIALS, 2017
VOL. 18, NO. 1, 563–573
https://doi.org/10.1080/14686996.2017.1360752

Taylor & Francis
Taylor & Francis Group

New intelligent multifunctional SiO_2/VO_2 composite films with enhanced infrared light regulation performance, solar modulation capability, and superhydrophobicity

Chao Wang[a,b], Li Zhao[a,b], Zihui Liang[a,b], Binghai Dong[a,b], Li Wan[a,b] and Shimin Wang[a,b]

[a]Hubei Collaborative Innovation Center for Advanced Organic Chemical Materials, Wuhan, PR China;
[b]Faculty of Materials Science and Engineering, Ministry of Education Key Laboratory for the Green Preparation and Application of Functional Materials, Hubei University, Wuhan, PR China

ABSTRACT

Highly transparent, energy-saving, and superhydrophobic nanostructured SiO_2/VO_2 composite films have been fabricated using a sol–gel method. These composite films are composed of an underlying infrared (IR)-regulating VO_2 layer and a top protective layer that consists of SiO_2 nanoparticles. Experimental results showed that the composite structure could enhance the IR light regulation performance, solar modulation capability, and hydrophobicity of the pristine VO_2 layer. The transmittance of the composite films in visible region (T_{lum}) was higher than 60%, which was sufficient to meet the requirements of glass lighting. Compared with pristine VO_2 films and tungsten-doped VO_2 film, the near IR control capability of the composite films was enhanced by 13.9% and 22.1%, respectively, whereas their solar modulation capability was enhanced by 10.9% and 22.9%, respectively. The water contact angles of the SiO_2/VO_2 composite films were over 150°, indicating superhydrophobicity. The transparent superhydrophobic surface exhibited a high stability toward illumination as all the films retained their initial superhydrophobicity even after exposure to 365 nm light with an intensity of 160 mW·cm^{-2} for 10 h. In addition, the films possessed anti-oxidation and anti-acid properties. These characteristics are highly advantageous for intelligent windows or solar cell applications, given that they can provide surfaces with anti-fogging, rainproofing, and self-cleaning effects. Our technique offers a simple and low-cost solution to the development of stable and visible light transparent superhydrophobic surfaces for industrial applications.

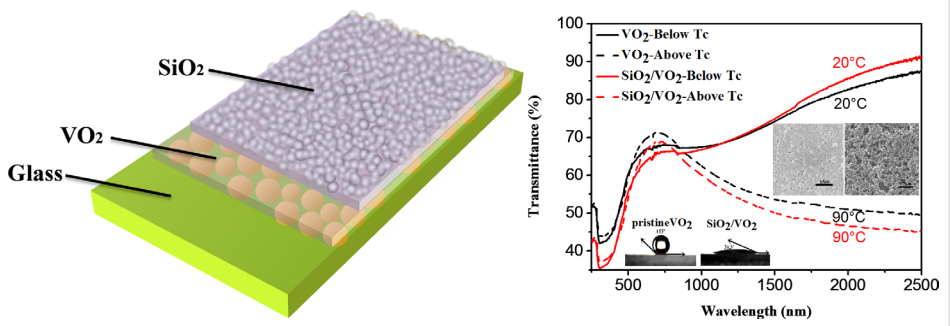

ARTICLE HISTORY
Received 12 June 2017
Revised 24 July 2017
Accepted 25 July 2017

KEYWORDS
Intelligent SiO_2/VO_2 composite films; IR-regulating; anti-oxidation; anti-acid; superhydrophobic

CLASSIFICATION
10 Engineering and Structural materials; 103 Composites; 204 Optics / Optical applications; 306 Thin film / Coatings

1. Introduction

The potential application of VO_2 thin films to intelligent windows has received considerable attention because of the over-increasing consumption of primary energy sources in recent decades [1–3]. VO_2 is a typical material with good thermal phase transition characteristics and has been widely used in intelligent windows [4]. VO_2 can adjust the inflow of solar heat by switching transmittance in the infrared (IR) region (780–2500 nm) while maintaining visible transmittance. The crystal structure of VO_2 is monoclinic (M phase) when its transition temperature (T_C) is higher than room temperature. As IR light and visible light have higher transmittance, room temperature will gradually increase as light enters. However, the crystal structure of VO_2 becomes tetragonal rutile (R phase) when its T_C is lower than room temperature. The transmittance of visible light remains constant, whereas the transmittance of IR light is reduced. Consequently, the heat generated by IR light cannot enter the room [5,6]. The aforementioned

CONTACT Li Zhao zhaoli7376@163.com; Shimin Wang shiminwang@126.com

phenomenon allows selectively controlling different wavelengths of light entering a room according to indoor temperature. This process does not require any other forms of external energy to drive intelligent temperature control. VO_2 is the first choice as material for intelligent temperature control due to the abrupt change in its optical properties before and after phase change. However, the main obstacles to the large-scale application of VO_2 films include decreasing phase transition temperature [7,8], enhancing visible light transmittance [9], increasing solar conditioning capacity [10] under strong visible light absorption conditions [11], and maintaining long-term stability upon exposure to air for a long period [12,13] or under high temperatures (above 300 °C) [14].

Metal ion doping of VO_2 thin films and the preparation of effective composite films are two main strategies for reducing phase transition temperature and improving transmittance, regulation rate, and anti-oxidant capacity of VO_2 thin film. The phase transition temperature of VO_2 thin films is effectively reduced to room temperature through ion doping. Metal ion doping of VO_2 thin films is an effective approach to reduce T_C. It mainly involves doping with cations and anions, such as tungsten [15,16], molybdenum [17], silicon [18], fluorine [19,20], niobium [21], and lanthanum [22]. Among these dopants, tungsten is most effective, lowering T_C by 20 °C per 1 at% [15]. VO_2 thin films can be co-doped with mixed metal ions, such as tungsten and molybdenum [23], tungsten and magnesium [24], and tungsten and fluorine [25]. A VO_2 thin film doped with lanthanum was prepared by Wang et al. Below 3 at% La doping level, the band gap (E_g) decreased steadily with the increase of dopant concentration. The 4 at% La-doped sample showed the best combination of T_{lum} 50.1% and ΔT_{sol} 10.3%, compared with other reported VO_2 continuous thin films [22]. Tungsten-doped VO_2 films have been prepared by a sol–gel method in our group. The phase transition temperature was further reduced to 32 °C, which was sufficient to meet the practical requirements [26]. A composite film typically contains three layers: the buffer layer, the functional layer, and the reinforcement layer. The buffer layer is primarily designed to improve the mechanical properties of a film, including its adhesion to glass as well as its hardness and stress [27]. Si_3N_4 and TiO_2 are the primary buffer layers used [28]. The functional layer refers to pristine or doped VO_2 films that exhibit typical thermal phase transition properties. The reinforcement layer, which can also be called anti-reflective layer, is mainly designed to increase the transmittance of light [29] and improve anti-oxidation and anti-acid properties [30]. TiO_2 [31], SiO_2 [12], and ZrO_2 [32] are the primary anti-reflective layers used. The low visible light transmittance of VO_2 thin films is mainly due to their intrinsic absorption and light reflection. As the refractive index of VO_2 thin films in the visible region and their reflectivity are high, the anti-reflective design of composite films must be enhanced.

Much research has been devoted to the fabrication of VO_2-based composite films on glass or flexible substrates aiming to increase the visible range transmittance. However, progress toward the optimization of one factor always comes at the expense of the other. Yu et al. fabricated the SiO_2/VO_2 composite films with a T_{lum} improved from 37.6% to 47.7%, while ΔT_{sol} exhibited a decrease from 8.06% to 7.62% via radio frequency (RF) sputtering and chemical vapor deposition, and the near-infrared (NIR) control capability was obviously decreased as well [33]. VO_2 thin film based on silicon–aluminum was prepared by Liu et al., in which the transmittance of the visible region was significantly enhanced (22% for T_{lum}), whereas the NIR control capability was slightly decreased [34]. There were only a few reports on the fabrication of VO_2-based composite films with enhanced solar conditioning capacity. Powell et al. fabricated the $VO_2/SiO_2/TiO_2$ composite films by chemical vapor deposition. The deposition of the SiO_2/TiO_2 overlayer resulted in a dramatic improvement of visible light transmission whilst also doubling the solar modulation of the material. However, the highest visible light transmittance was still below 60%, which was not sufficient to meet the requirements of glass lighting [35]. In addition, nanoporous films [36], biomimetic moth-eye structures [37], and micro-grid structures [38] are three major nanostructuring approaches to enhance both T_{lum} and ΔT_{sol} of VO_2 films. Micro-patterned VO_2 films were fabricated by Lu et al. using a facile screen printing method; the best performing sample gave 43.3% T_{lum} and 14.9% ΔT_{sol}, which were comparable to most approaches used to enhance thermochromic properties [38].

Superhydrophobic surfaces, such as composite films on glasses and metals, have many unique properties, such as self-cleaning, anti-sticking, anti-icing, anti-biofouling, water and bacteria proofing, drag reduction, and humidity proofing [39–43]. In the present study, intelligent multifunctional SiO_2/VO_2 composite films were fabricated using the sol–gel method. These composite films are composed of an underlying infrared (IR)-regulating VO_2 layer and a top SiO_2 protective layer that is deposited with SiO_2 nanoparticles. They differ from a conventional approach, which includes a solid reinforcing layer. The accumulation of SiO_2 nanoparticles in the film constitutes a highly porous nanoscale network structure, and the deposited SiO_2 thin films has low surface energy, which renders excellent superhydrophobicity and self-cleaning properties. In addition, nanosilica with small particles provided a coarse micro-nanostructure by stacking the surfaces, thereby promoting reduction in the reflectivity of composite films. While maintaining the outstanding optical transmittance which was higher than 60% of VO_2 film, the solar control ability of composite film is greatly improved. The experimental results showed an interesting phenomenon, i.e. both NIR control capability and solar modulation capability were simultaneously enhanced. This phenomenon provides

a new avenue toward enhancing the visible light transmittance and solar energy regulation capacity of VO_2 thin films. Our technique offers a simple and low-cost solution to the development of stable and highly visible light transparent composite films for potential industrial applications.

2. Experimental section

2.1. Materials and chemicals

The following were used: vanadyl acetylacetonate ($C_{10}H_{14}O_5V$, 98% AR, purchased from Aladdin Reagent Co. Ltd, Shanghai, China), tungsten(VI) chloride (WCl_6, 98% AR, purchased from Aladdin Reagent Co. Ltd, Shanghai, China), methanol (CH_4O, 99.5% AR, purchased from Chinese Sinopharm Chemical Reagent Co. Ltd, Shanghai, China), trimethoxymethylsilane ($C_4H_{12}O_3Si$, 98% AR, purchased from Aladdin Reagent Co. Ltd, Shanghai, China), oxalic acid dihydrate ($C_2H_4{\cdot}2H_2O$, 99.5% AR, purchased from Aladdin Reagent Co. Ltd, Shanghai, China), ammonia solution (NH_3, 25%~28% AR, purchased from Chinese Sinopharm Chemical Reagent Co. Ltd, Shanghai, China).

2.2. Preparation of tungsten-doped VO_2 films

The VO_2 precursor was prepared using a sol–gel method, followed by a typical synthesis procedure. Then, 1.00 g commercial vanadyl acetylacetonate and quantitative WCl_6 were dissolved in 30 mL methanol with vigorous constant stirring in a 50 mL glass beaker for 24 h to ensure that $VO(acac)_2$ was dissolved and formed a dark brown solution with a concentration of 0.125 mol·L^{-1}. The VO_2 precursor was formed after aging for 48 h. Simultaneously, fused quartz with the dimensions of 2 cm × 2 cm × 1 mm was prepared after cleaning consecutively with deionized (DI) water, ethanol, and acetone. This fused quartz was used as the substrate for depositing VO_2 films. The VO_2 precursor was spin-coated on the fused quartz with a low rate of 800 rpm for 9 s and a high rate of 2500 rpm for 30 s. Then, the sample was dried in a vacuum oven at 100 °C for 30 min to remove excess solvent. The deposition processes of spin-coating and drying in a cyclic fashion were repeated three times, which was marked as (VO_2) *3. Finally, the samples were annealed at 600 °C for an hour under argon atmosphere through a programmed sintering process.

2.3. Preparation of SiO_2 gels

Gels were obtained via a two-step acid-base catalysis mechanism. In this process, 1 mL of trimethoxymethylsilane and 0.5 mL of 0.001 M oxalic acid solution were dissolved in 10 mL methanol with vigorous constant stirring for 3 h. After hydrolysis, 0.61 mL of 11.2 M ammonium hydroxide solution was added dropwise to the reaction mixture to catalyze the condensation reaction. Then, the reaction mixture was stirred for 30 min, and the solution was left for gelation and aging for 24 h at room temperature.

2.4. Preparation of SiO_2/VO_2 composite films

The resulting gels were diluted and homogenized with 25 mL methanol using an ultrasonic liquid homogenizer for 30 min. The obtained homogenized solutions were spin-coated on fused quartz for different times (n) in which VO_2 films had been successfully spin-coated at a low rate of 1000 rpm for 9 s and a high rate of 3000 rpm for 30 s, then the SiO_2/VO_2 composite films were marked as (SiO_2) *n /(VO_2) *3. Then, the samples were dried in a vacuum oven at 100 °C for 30 min to remove excess solvent and organic groups. The deposition processes of spin-coating and drying in a cyclic fashion were repeated three times. Finally, the samples were annealed at 450 °C for an hour under argon atmosphere through a programmed sintering process.

2.5. Characterization

The surface morphologies of the composite films were studied using a JSM-5610LV scanning electron microscope (SEM) (JEOL, Akishima-shi, Tokyo, Japan) at an accelerating voltage of 20 kV. All the samples were coated with gold using a commercial sputtering apparatus prior to SEM measurements. The ultraviolet (UV)–visible diffuse reflectance spectra of the SiO_2/VO_2 composite films were measured with a UV–visible spectrophotometer (UV-3600, Shimadzu Corporation, Tokyo, Japan) at normal incidence. The samples obtained were characterized via X-ray diffraction (XRD) using a D/MAX-IIIC X-ray diffractometer (Akishima-shi, Tokyo, Japan) with Cu Kα radiation (λ = 0.15406 nm) to determine the phase structures and crystallite sizes of the samples obtained. The water contact angle of SiO_2/VO_2 composite films was measured via the sessile drop technique using a KRUSS DSA100 (Shanghai Xuan Yi Chong Industrial Equipment Co. Ltd., Shanghai, China) contact angle system, with DI water drops of approximately 15 μL applied to three different spots for each coating. Atomic force microscopy (AFM) images were collected using a Park Systems XE-100 (Suwon, Korea) operating in noncontact mode.

3. Results and discussion

3.1. Morphologies of tungsten-doped VO_2 films and SiO_2/VO_2 composite films

Figure 1 shows the SEM and AFM images of the surface morphologies of tungsten-doped VO_2 films and SiO_2/VO_2 composite films on quartz after calcination. For tungsten-doped VO_2 films, the mean grain size and

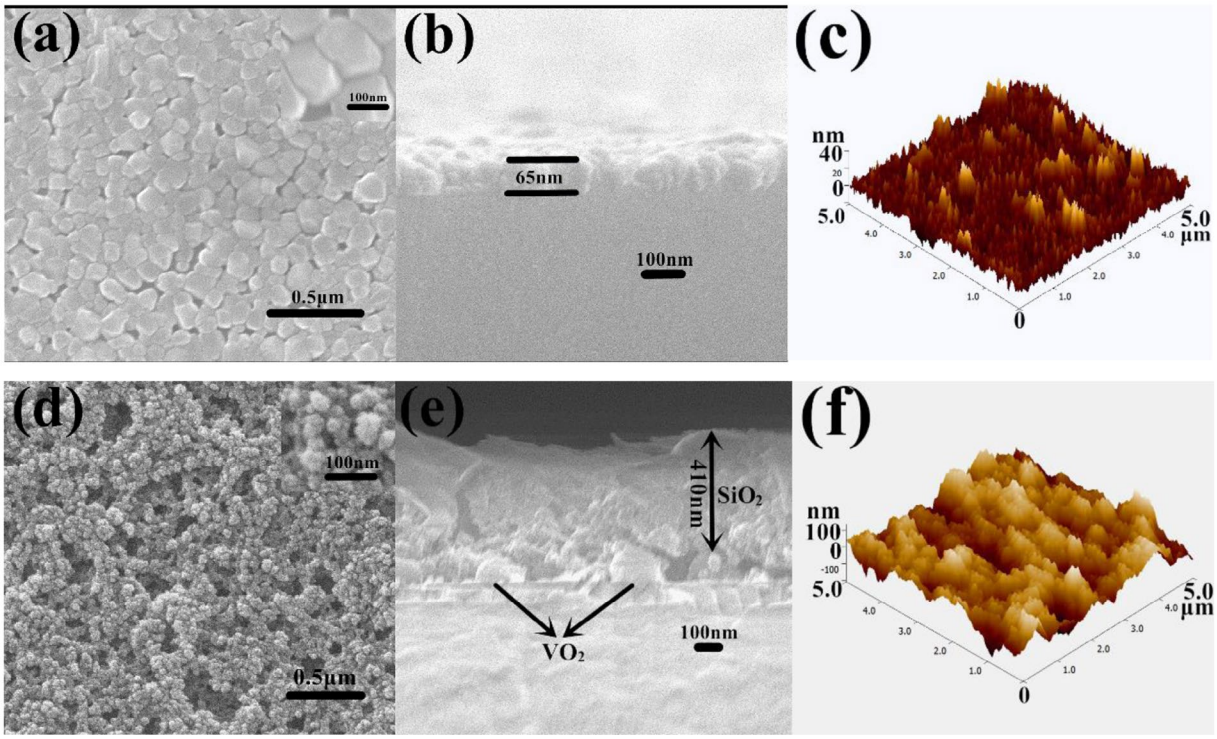

Figure 1. SEM and AFM images of tungsten-doped VO_2 films (a)–(c) and SiO_2/VO_2 composite films (d)–(f) on quartz after calcination.

thickness of tungsten-doped VO_2 films deposited on the quartz substrate were approximately 100 nm (Figure 1(a)) and 65 nm (Figure 1(b)), respectively. The surface roughness value of tungsten-doped VO_2 was 20.5 nm (Figure 1(c)). Most of the particles were spherical, whereas others were larger oval. The particles were dispersed evenly and densely on the surface. The smallest particle was approximately 50 nm, whereas the largest was approximately 150 nm. We calculated grain size according to the Debye–Scherrer formula [44,45]. The particle sizes of tungsten-doped VO_2 nanoparticles with different volumes of tungsten, calculated from the width of the 110 reflection, ranged from 20 to 120 nm [26]. We chose a suitable thickness, namely, three layers of spin coating, to improve the optical effect. Increasing the thickness of tungsten-doped VO_2 films can strengthen the IR-regulating capability of composite films. However, the transmittance in the visible region is significantly reduced [46]. Nevertheless, parts of the surface were still visible, which indicated that the substrate was not fully covered. The optical effect will be enhanced if particle surface coverage is improved. As shown in Figure 1(d), the surface morphologies of SiO_2/VO_2 composite films have highly porous networks. We can obtain porosity by controlling the amount of methanol. The annealed tungsten-doped VO_2 spherical particles and SiO_2 film were marked in the electron micrograph. The size of the spherical VO_2 particles is approximately 100 nm, which is consistent with the results of the SEM test and the theoretical calculations. The thickness of SiO_2 film is approximately 410 nm, and 478 nm is the total film thickness (Figure 1(e)). The surface roughness value of SiO_2/VO_2 composite films is 44.0 nm (Figure 1(f)), which is higher than that of tungsten-doped VO_2 films. The SiO_2 nanoparticles are relatively uniform, and particle size is smaller than that of VO_2. The results obtained suggest that the voids between spherical tungsten-doped VO_2 particles have been filled with SiO_2 nanoparticles.

3.2. IR-regulating property of VO_2 films and SiO_2/VO_2 composite films

Figure 2(a1) shows the transmittance spectra, hysteresis loops at 2000 nm (a2), and corresponding d(Tr)/d(T)&T curve (a3) for pristine VO_2 and SiO_2/VO_2 composite films, as well as the transmittance spectra (b1), hysteresis loops at 2000 nm (b2), and corresponding d(Tr)/d(T)&T curve (b3) for tungsten-doped VO_2 and SiO_2/VO_2 composite films. As shown in Figure 2(a1) and (b1), all samples change their transmittance spectra upon heating from 20 °C to 90 °C. The metal–insulator transition (MIT) of VO_2 was observed and accompanied by an abrupt change in IR transmittance. The near-infrared switching efficiency (NIRSE) of SiO_2/VO_2 composite films (35.5%) was remarkably higher than that of pristine VO_2 films (30%), although the SiO_2/VO_2 film was thicker. This enhancement can be attributed to two factors. First, the size of SiO_2 nanoparticles was approximately 20 nm, which was considerably smaller than the size of the visible light wavelength. The degree of decrease in transmittance and loss of light posed negligible effects. The size of SiO_2 particles was significantly smaller than that of VO_2 particles, and the voids between spherical VO_2 particles were filled with SiO_2

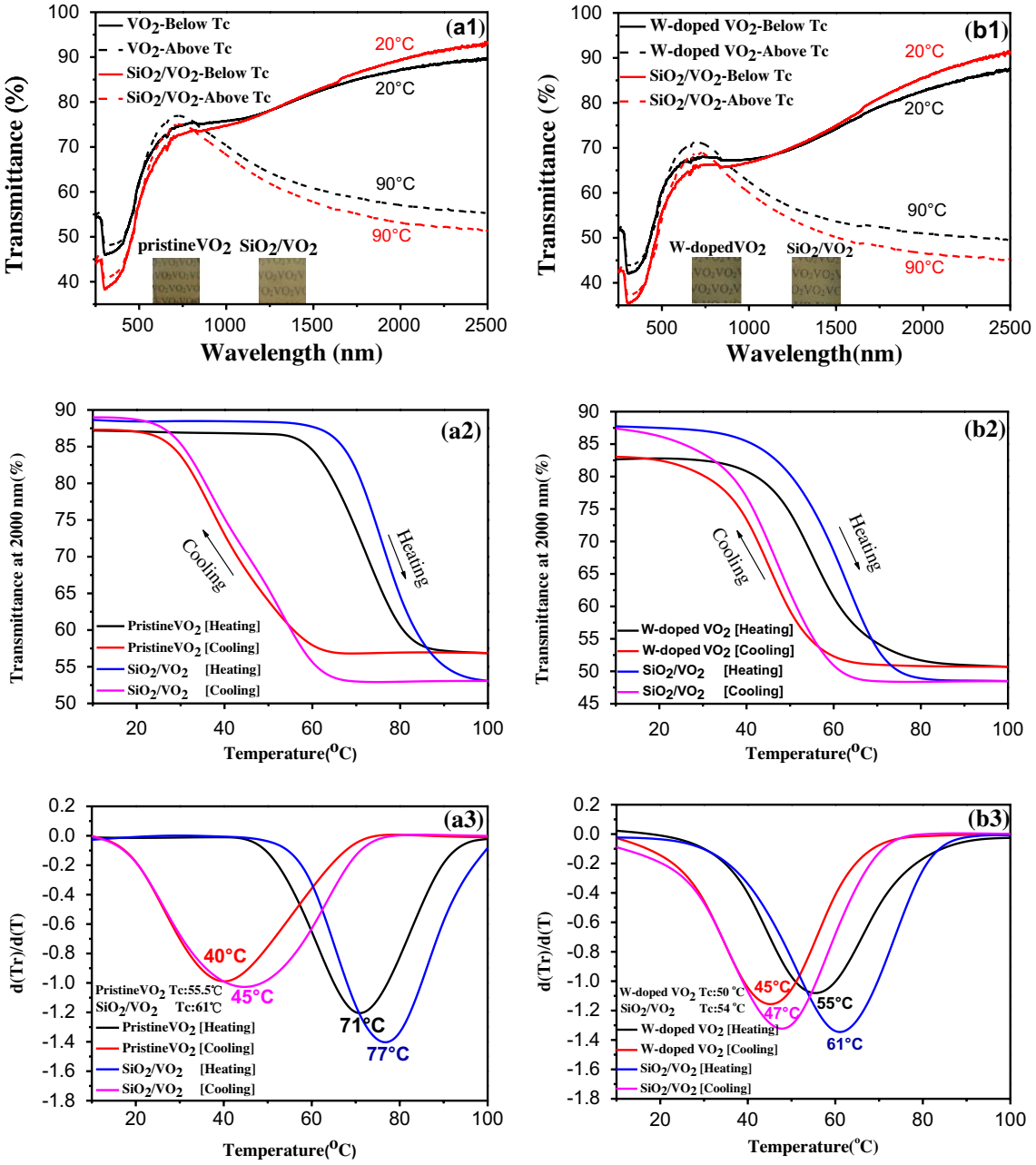

Figure 2. Transmittance spectra (a1), hysteresis loops at 2000 nm (a2), (a)--(c)corresponding d(Tr)/d(T)&T curve (a3) for pristine VO_2 and SiO_2/VO_2 composite films. Transmittance spectra (b1), hysteresis loops at 2000 nm (b2), and corresponding d(Tr)/d(T)&T curve (b3) for tungsten-doped VO_2 and SiO_2/VO_2 composite films.

nanoparticles. Nanosilica with small particles provided a coarse micro-nanostructure by stacking the surfaces, thereby promoting reduction in the reflectivity of composite films and improving the total amount of sunlight passing through the composite films, as shown in Figure 3(a). Consequently, the NIR control capability of composite films was enhanced. This result shows potential value in promoting SiO_2/VO_2 composite films. To fully display the superior optical properties of SiO_2/VO_2 composite films, the visible transmittance (T_{lum}, 380–780 nm) and solar spectral transmittance (T_{sol}, 300–2500 nm) of all the films were calculated according to standard spectra [47] and Equation (1) [48] for the prepared VO_2 thin films and SiO_2/VO_2 composite films:

$$T_{lum/sol} = f\psi_{lum/sol}(\lambda)T(\lambda)d(\lambda)/f\psi_{lum/sol}(\lambda)d(\lambda) \quad (1)$$

where $T(\lambda)$ corresponds to the transmittance at the transmission wavelength λ, ψ_{lum} denotes the standard luminous efficiency function for the photopic vision of the human eyes, and the wavelength range of $T(\lambda)$ measures 380–780 nm; ψ_{sol} refers to solar spectral irradiance that corresponds to an atmospheric mass of 1.5. The angle between the sun and the horizon is above 37°, and the wavelength of $T(\lambda)$ ranges from 300 nm to 2500 nm. Luminous transmittance modulation (ΔT_{lum}) and solar energy modulation (ΔT_{sol}) are defined as follows:

$$\Delta T_{lum} = T_{lum,s} T_{lum,m}, \quad (2)$$

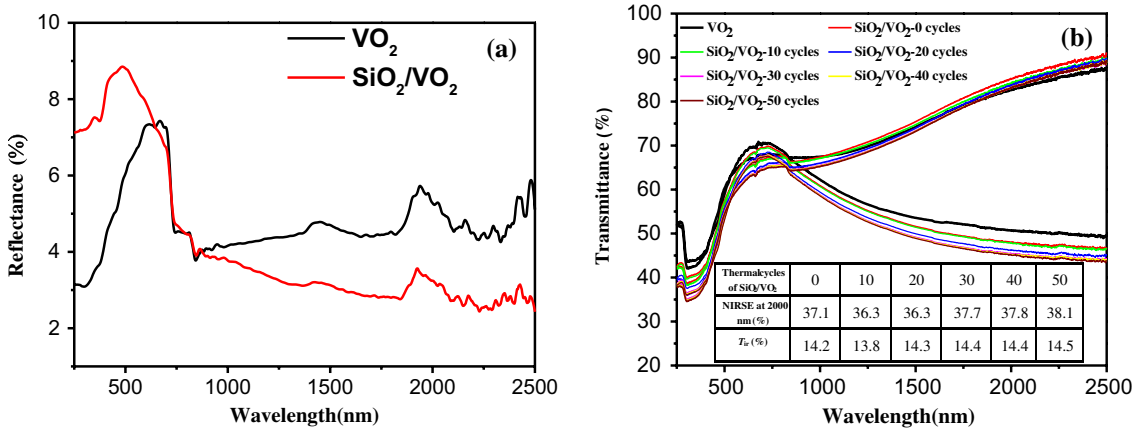

Figure 3. Reflectance spectra for pristine VO_2 and SiO_2/VO_2 composite films (a). Transmittance spectra for SiO_2/VO_2 composite films subjected to thermal cycling (b).

Table 1. Solar energy modulation parameters of pristine VO_2 film and SiO_2/VO_2 composite films.

W/(W+V) molar ratio (%)		$T_{lum,s}$ (%)	$T_{lum,m}$ (%)	$T_{sol,s}$ (%)	$T_{sol,m}$ (%)	ΔT_{sol} (%)	NIRSE at 2000 nm (%)	T_{ir} (%)	ΔT_C (°)	T_C (°)
0	pristine VO_2	67.5	68.9	70.2	65.6	4.6	30	12.2	31.1	55.3
	SiO_2/VO_2	63.3	65.2	67.3	62.2	5.1	35.5	13.9	32.2	60.6
0.5	pristine VO_2	64	64.8	64.7	59.5	4.8	31.7	12.2	10.4	50.4
	SiO_2/VO_2	60.1	61.2	62.5	56.6	5.9	39	14.9	13.4	54.3

$$\Delta T_{sol} = T_{sol,s} T_{sol,m}. \quad (3)$$

$T_{lum,s}$ and $T_{lum,m}$ indicate the luminous transmittance of films in semiconductor and metal states, respectively. $T_{sol,s}$ and $T_{sol,m}$ indicate the solar transmittance of films in semiconductor and metallic states, respectively. MIT temperature was defined as $T_C = (T_1 + T_2)/2$, and the width of the hysteresis loop was described by $\Delta T = T_1 - T_2$. Table 1 presents all the results obtained. ΔT_{sol} was 4.6% for pristine VO_2 film, the hysteresis width (ΔT_C) reached 31 °C, and the transition temperature (T_C) was measured to be 55.5 °C, which was lower than the classical 67 °C for pristine VO_2. These results were attributed to the size effect of nanoparticles: more grain boundaries and film defects occurred with small particle size, and surface energy was sufficiently high to decrease the activation energy and the energy barrier. Thus, the phase change and reverse-phase transition proceeded easily [49,50]. The actual phase transition temperature decreased. ΔT_{sol} reached 5.1%, the hysteresis width (ΔT_C) measured 32 °C, and the transition temperature (T_C) was 61 °C for SiO_2/VO_2 composite films. For tungsten-doped VO_2 films, ΔT_{sol} reached 4.8% and 5.9% for VO_2 films and SiO_2/VO_2 composite films, the hysteresis width (ΔT_C) measured 10 °C and 14 °C, and the transition temperature (T_C) was 50 °C and 54 °C, respectively, which were considerably lower than the classical 67 °C for pristine VO_2. Three theories have been proposed to explain the reduced phase transition temperature caused by element doping: theory of length [51], theory of charge transfer [52], and stress theory [53].

It was obvious that the VO_2 thin films doped with a metal ion did not change the characteristic of enhancing the near IR control capability of the composite film shown in Table 1. The phase transition temperature of VO_2 films could be reduced by controlling the amount and type of metal ion. That made it possible to reduce the phase transition temperature and improve the infrared modulation ability for the composite films simultaneously. The aforementioned results demonstrated that SiO_2/VO_2 composite films showed excellent thermochromic properties similar to those of VO_2 films, and the solar modulation capability of VO_2 films improved significantly. Doping with tungsten significantly affected the phase transition temperature of VO_2. For example, when doping amount reached 0.5%, the phase transition temperature of the products was decreased to 50 °C. However, when doping amount increased to 1.5% [26], the phase transition temperature was further reduced to 32 °C. Simultaneously, the hysteresis width of the film was reduced effectively by tungsten doping and SiO_2/VO_2 composite films.

A thermal cycling test was performed to study the cycling stability of SiO_2/VO_2 composite films in terms of IR regulation. The quartz glass coated with SiO_2/VO_2 composite films was thermally cycled between 0 °C and 100 °C on a heating platform. The UV transmittance of composite films was measured after every 10 cycles, and the results are shown in Figure 3(b). The NIRSE of SiO_2/VO_2 composite films at 2000 nm decreased slightly at 10th and 20th thermal cycles, but showed a marked increase at 30th to 50th cycles. The NIR control capability of composite films also enhanced slightly; however, the overall transmittance of composite films reduced slightly. The UV transmittance of composite

films was measured after 24 h, and the NIR transmittance of composite films increased, with a NIRSE of 40.7% (at 2000 nm); meanwhile the NIR control capability was 16%. The enhancement can be attributed to the improved crystallinity of VO_2 under the condition of continuous thermal cycling, which resulted in a better infrared modulation.

3.3. Anti-oxidation and anti-acid properties of SiO_2/VO_2 composite films

The structures of SiO_2/VO_2 composite films effectively enhanced the anti-oxidation and acid-resisting properties of pristine VO_2 films. SiO_2 film was used not only used as anti-reflective layer but also as a barrier for oxygen diffusion to effectively prevent VO_2 from being oxidized to V_2O_5 or other high valence vanadium oxides. This assumption was confirmed by a comparative study of uncoated and coated SiO_2 nanoparticles after exposing them to air for 1 month at room temperature.

As shown in Figure 4(a) and (b), the MIT of pristine VO_2 films was observed and accompanied by an abrupt change in IR transmittance. The NIRSE of pristine VO_2 films and SiO_2/VO_2 composite films was 34.0% and 35.7% at 2000 nm for Sample I and Sample III, while the NIRSE was 17.8% and 35.5% for Sample II and Sample IV after air exposure for 1 month at room temperature. NIRSE was reduced by about 47.6% for the uncoated VO_2 films, whereas it changed slightly in SiO_2/VO_2 composite films. Evidently, VO_2 films underwent vanadium oxide reaction and were oxidized to V_2O_5 or other high valence vanadium oxides in air [12]. VO_2 particles can be effectively prevented from being oxidized to other high valence vanadium oxides by adding a layer of SiO_2 on the VO_2 film as a barrier layer for oxygen diffusion.

Figure 5(a) shows the XRD patterns of uncoated VO_2 films (black line) and SiO_2/VO_2 composite films (red line), and Figure 5(b) shows transmittance spectra at 500 nm of uncoated VO_2 and SiO_2/VO_2 composite films in acidic solution at different durations. The XRD signals are relatively weak due to the nanocrystalline structure and small thickness of the films. The peaks at 27.9° and 57.7° were ascribed to the (011) and (022) planes, respectively, of monoclinic VO_2 (JCPDS No. 82–0661), which were observed in pristine VO_2 films. However, the peak intensity at 27.9° visibly decreased, and the peak at 57.7° disappeared due to the destruction of the SiO_2 layer in SiO_2/VO_2 composite films. Moreover, no significant diffraction peaks were observed for other vanadium oxides.

An acid corrosion resistance test was carried out to study the corrosion resistance of SiO_2/VO_2 composite films. An equal amount of hydrochloric acid solution was added to uncoated VO_2 and SiO_2/VO_2 composite films at room temperature. The hydrochloric acid solution (pH = 1) was selected to accelerate film erosion and to ease observation. During acid erosion, we directly observed that the surface of uncoated VO_2 films quickly dissolved, and film color changed from dark brown to light yellow. In contrast, SiO_2/VO_2 films did not show visible color changes after the first 10 min. The surface of SiO_2/VO_2 composite films appeared as light brown patches at 10 to 20 min, thereby indicating that the superhydrophobic SiO_2 film was partially destroyed leading to the corrosion of VO_2 film. After 30 min, VO_2 film was completely dissolved, whereas some unbroken SiO_2 film remained on the glass substrate surface. Figure 5(b) shows film transmittance at 500 nm after different exposure times to the same acid. The curve clearly shows that the transmittance of uncoated VO_2 film rapidly increased from 25.7% to 73.0% after 400 s of acidic treatment. However, the transmittance of SiO_2/VO_2 composite films increased from 24.7% to 30.8%. The results indicate that SiO_2/VO_2 composite films can withstand acidic treatment due to the protection of the SiO_2 hydrophobic layer.

3.4. Superhydrophobic surfaces of SiO_2/VO_2 composite films

Figure 6 shows SEM and AFM images of VO_2 films and SiO_2/VO_2 composite films on quartz after calcination. The SEM images showed that all the membranes

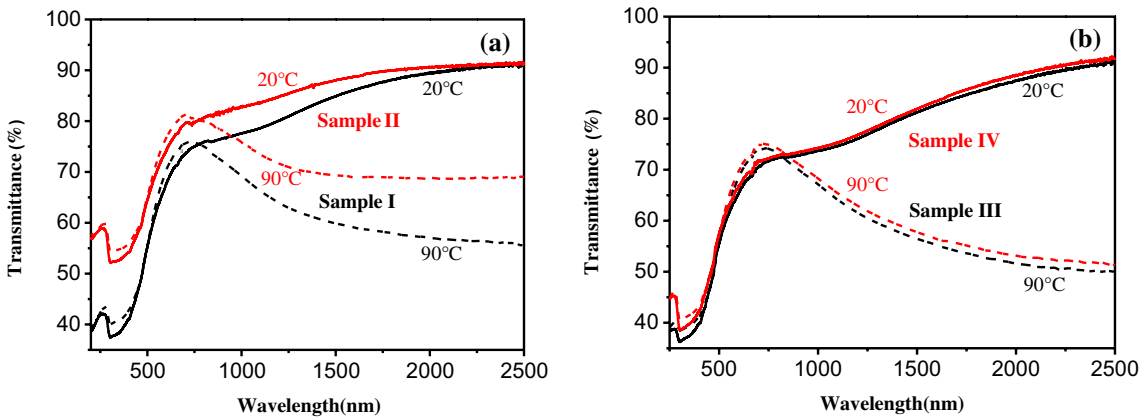

Figure 4. Transmittance spectra of pristine VO_2 films (a) and SiO_2/VO_2 composite films (b) before and after treatment with air for 1 month at room temperature.

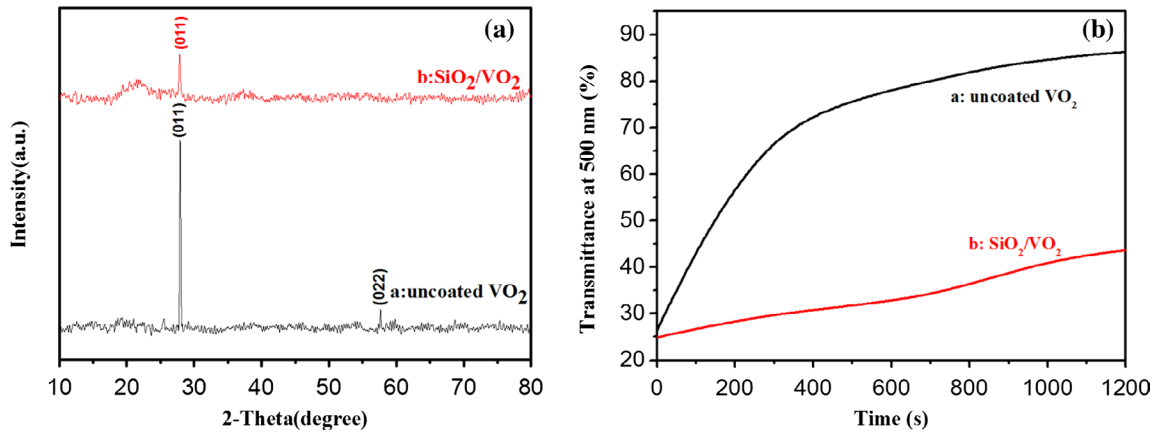

Figure 5. XRD patterns of the pristine uncoated VO_2 and SiO_2/VO_2 composite films (a). Transmittance spectra at 500 nm of the pristine uncoated VO_2 and SiO_2/VO_2 composite films in acidic solution at different times (b).

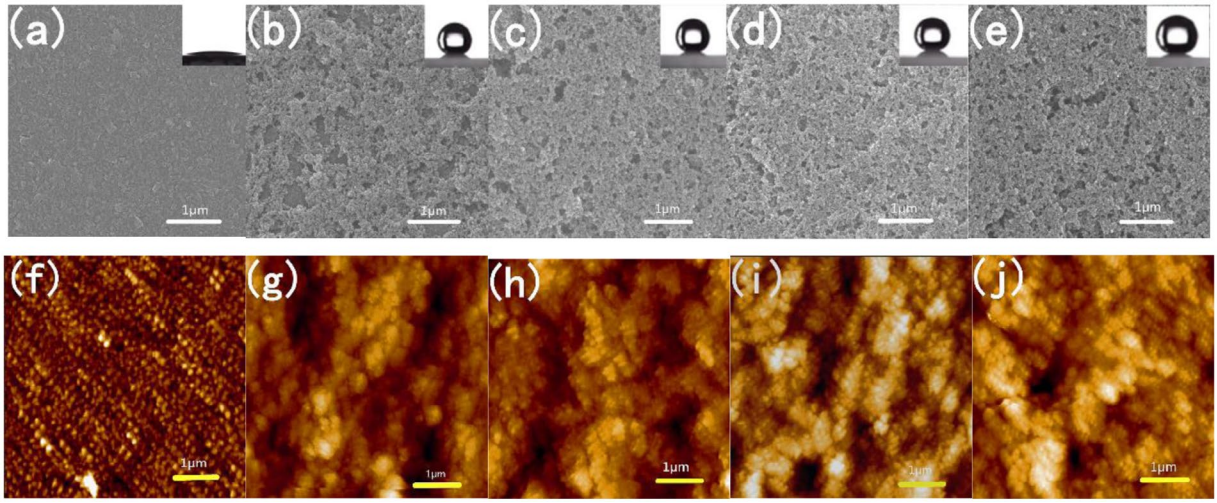

Figure 6. SEM micrographs of VO_2 (a) and SiO_2/VO_2 composite (b)–(e) films. AFM images of VO_2 (f) and SiO_2/VO_2 composite (g)–(j) films on quartz after calcination. (a) (VO_2) *3, (b) (SiO_2) *1/(VO_2) *3, (c) (SiO_2) *2/(VO_2) *3, (d) (SiO_2) *3/(VO_2) *3, and (e) (SiO_2) *4/(VO_2) *3. Insets show images of the water contact angle of the corresponding films.

featured a highly nanoporous network structure and were deposited with spherical SiO_2 particles with a size of 20 nm. Porosity was determined by controlling the amount of methanol [54,55]. The water contact angle of the surface is related to both surface energy and roughness [56,57]. The combination of micrometer- and nanometer-sized pores induced superhydrophobicity. Within a certain range, higher porosity resulted in increased static contact angle. Increasing roughness allowed the entrapment of more air between the water and the surface. The surface roughness of the nanostructure composite films decreased with an increase in SiO_2 layers before gradually stabilizing. As shown in Figure 7(a) and (b), the average surface roughness of pure VO_2 films was 6.2 nm, which was significantly lower than that of SiO_2/VO_2 composite films. Consequently, pure VO_2 thin films exhibited a smaller water contact angle, which was hydrophilic. The average roughness of SiO_2/VO_2 composite films was much higher than VO_2 thin films, which was sufficient to meet the requirements of roughness of superhydrophobicity. It is well known that methytrimethoxysilane is a common silane coupling agent, and the surface of SiO_2 nanoparticles (formed during the reaction after the methytrimethoxysilane was decomposed) were modified simultaneously. The combination of micrometer- and nanometer-sized pores and low surface energy induced superhydrophobicity.

The average roughness of SiO_2/VO_2 composite films with one spun layer was highest, and it was the most prone to failing full coverage of VO_2 films. Consequently, the water contact angle was less than 150°. With the increase in the number of spin-coated SiO_2 layers, the water contact angle of composite films reached 155°, whereas average roughness stabilized at 40 nm, which was highly suitable for the use of transparent superhydrophobic composite films for glazing. However, scattering of light by these films increased remarkably, whereas transmittance was reduced significantly when surface roughness was higher than 100 nm [58]. Hence, it was not conducive to the application and promotion for SiO_2/VO_2 composite films.

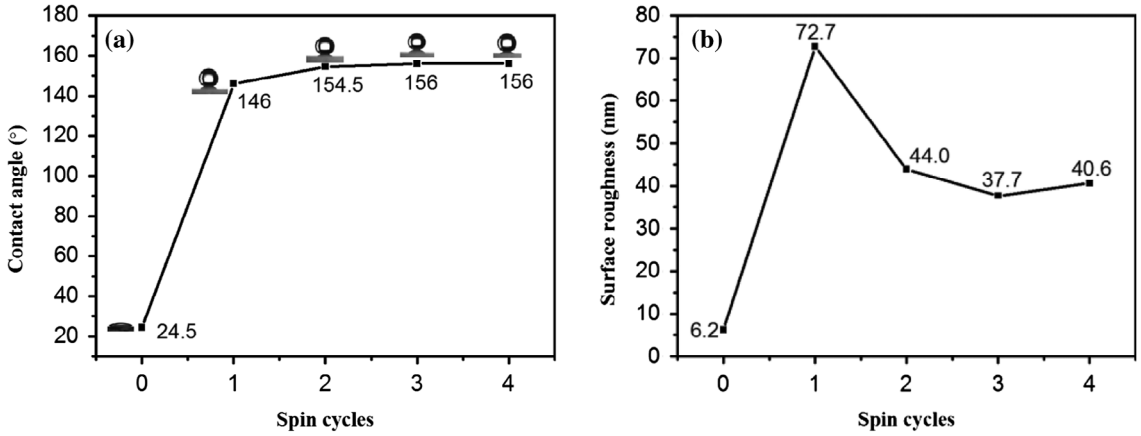

Figure 7. Water contact angles and average roughness of the composite films. The composite films were prepared from (VO_2) *3, (SiO_2) *1/(VO_2) *3, (SiO_2) *2/(VO_2) *3, (SiO_2) *3/(VO_2) *3, and (SiO_2) *4/(VO_2) *3.

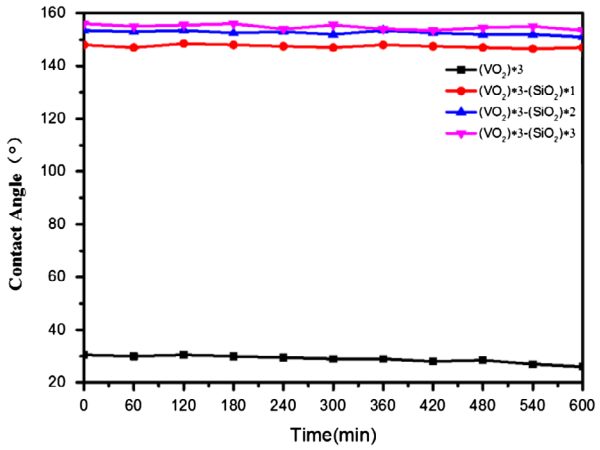

Figure 8. Changes in water contact angle of SiO_2/VO_2 composite films during irradiation with 160 mW·cm^{-2} UV light. Composite films were prepared from (VO_2) *3 (squares), (SiO_2) *1/(VO_2) *3 (circular dots), (SiO_2) *2/(VO_2) *3 (blue triangles), and (SiO_2) *3/(VO_2) *3 (pink triangles).

The UV stability of superhydrophobic surface was observed by comparing changes in the water contact angle on the coating surface. Figure 8 displays changes in the water contact angle of superhydrophobic SiO_2/VO_2 composite films under 365 nm illumination with an intensity of 160 mW·cm^{-2}. The water contact angle of VO_2 films was initially 30.5° and was hydrophilic, whereas the water contact angle of (SiO_2) *1/(VO_2) *3 reached 148° for failing to fully cover the VO_2 film. The water contact angles of (SiO_2) *2/(VO_2) *3 and (SiO_2) *3/(VO_2) *3 were 152.5° and 155°, respectively. The hydrophobic angles of the four films did not change with prolonging irradiation time with a UV lamp until irradiation time was extended to 10 h. The water contact angle of (VO_2) *3 film was reduced by 26.5°, and hydrophilicity was enhanced. VO_2 and TiO_2 are typical photosensitive semiconductor materials. Films exposed to UV light will produce photogenerated holes. The interaction between photogenerated holes and lattice oxygen will form oxygen vacancies on the surface of VO_2, and hydrogen bonds will be formed through the reaction of oxygen vacancies and water molecules, thereby enhancing the hydrophilicity of surfaces [59,60]. In contrast, the water contact angles of (SiO_2) *1/(VO_2) *3, (SiO_2) *2/(VO_2) *3, and (SiO_2) *3/(VO_2) *3 changed minimally; the hydrophobic angles were 147°, 152.5°, and 154.5°, respectively. Consequently, SiO_2/VO_2 composite films were not only superhydrophobic but also resistant to high-intensity UV illumination.

4. Conclusions

In this work, highly transparent, IR-regulating and superhydrophobic nanostructured SiO_2/VO_2 composite films were fabricated via a sol–gel approach. The composite films comprised an underlying IR-regulating VO_2 layer and a top protective layer that consists of SiO_2 nanoparticles. The composite films not only possessed excellent optical properties but also good hydrophobic features. The transmittance of the visible region was higher than 60%, which sufficiently meets requirements of glass lighting. The NIRSE reached 40% at 2000 nm, and the NIR control capability of the composite films was enhanced relatively by 13.9% and 22.1%, whereas the solar modulation capability was enhanced by 10.9% and 22.9%, respectively, in comparison with VO_2 films and tungsten-doped VO_2 thin films. The water contact angle of SiO_2/VO_2 was higher than 150°. The transparent superhydrophobic surfaces exhibited a high stability to illumination—all the films retained their initial superhydrophobicity even after exposure to 365 nm light with an intensity of 160 mW·cm^{-2} for 10 h. This composite structure improved the anti-oxidation and anti-acid properties of VO_2 films. The performances observed are advantageous for surface anti-fogging, rainproofing, and self-cleaning effects of the films studied. Our technique offers a simple and low-cost process for developing stable and visible light transparent superhydrophobic surfaces for industrial applications.

Disclosure statement

No potential conflict of interest was reported by the authors.

Funding

The work was supported by the National Natural Science Foundation of China [51572072; 21402045] and the PhD Programs Foundation of the Ministry of Education of China [20114208110004]. This work was also financially supported by the Wuhan Science and Technology Bureau of Hubei Province of China [2013010501010143], the Educational Commission of Hubei Province of China [D20141006], and the Department of Science and Technology of Hubei Province of China [2015CFA118; 2013CFA005].

References

[1] DoE US. Energy efficiency & renewable energy department. Buildings energy databook. 2011.
[2] Baetens R, Jelle BP, Gustavsen A. Properties, requirements and possibilities of smart windows for dynamic daylight and solar energy control in buildings: A state-of-the-art review. Sol Energ Mat Sol C. 2010;94(2):87–105.
[3] Fridley DG. Estimating total energy consumption and emissions of China's commercial and office buildings. California: Lawrence Berkeley National Laboratory. 2008.
[4] Park JH, Coy JM, Kasirga TS, et al. Measurement of a solid-state triple point at the metal-insulator transition in VO_2. Nature. 2013;500(7463):431–434.
[5] Wang M, Bian J, Sun H, et al. Sunlight-induced resistance changes and their effects on the semiconductor–metal transition behavior of VO_2 film. J Mater Sci. 2016;51(17):8233–8239.
[6] Bian J, Wang M, Miao L, et al. Growth and characterization of VO_2/p-GaN/sapphire heterostructure with phase transition properties. Appl Surf Sci. 2015;357:282–286.
[7] Rajeswaran B, Umarji AM. Effect of W addition on the electrical switching of VO_2 thin films. Aip Adv. 2016;6(3):035215.
[8] Fan LL, Chen S, Liao GM, et al. Comprehensive studies of interfacial strain and oxygen vacancy on metal–insulator transition of VO_2 film. J Phys-Condens Mat. 2016;28(25):255002.
[9] Kang L, Gao Y, Luo H, et al. Nanoporous thermochromic VO_2 films with low optical constants, enhanced luminous transmittance and thermochromic properties. ACS Appl Mater Inter. 2011;3(2):135–138.
[10] Ye H, Meng X, Xu B. Theoretical discussions of perfect window, ideal near infrared solar spectrum regulating window and current thermochromic window. Energ Buildings. 2012;49:164–172.
[11] Mlyuka NR, Niklasson GA, Granqvist CG. Thermochromic VO_2-based multilayer films with enhanced luminous transmittance and solar modulation. Phys Status Solidi A. 2009;206(9):2155–2160.
[12] Wang M, Tian J, Zhang H, et al. Novel synthesis of pure VO_2@ SiO_2 core@ shell nanoparticles to improve the optical and anti-oxidant properties of a VO_2 film. Rsc Adv. 2016;6(110):108286–108289.
[13] Lindström R, Maurice V, Zanna S, et al. Thin films of vanadium oxide grown on vanadium metal: oxidation conditions to produce V_2O_5 films for Li-intercalation applications and characterisation by XPS, AFM. RBS/NRA Surf Interfa Anal. 2006;38(1):6–18.
[14] Fu G, Polity A, Volbers N, et al. Annealing effects on VO_2 thin films deposited by reactive sputtering. Thin Solid Films. 2006;515(4):2519–2522.
[15] Peng Z, Wang Y, Du Y, et al. Phase transition and IR properties of tungsten-doped vanadium dioxide nanopowders. J Alloy Compd. 2009;480(2):537–540.
[16] Huang Z, Chen C, Lv C, et al. Tungsten-doped vanadium dioxide thin films on borosilicate glass for smart window application. J Alloy Compd. 2013;564:158–161.
[17] Phoempoon P, Sikong L. Synthesis of Thermochromic Mo-Doped VO_2 Particles. Mater Sci Forum. 2016;867:88–92.
[18] Zhang H, Wu Z, Niu R, et al. Metal–insulator transition properties of sputtered silicon-doped and un-doped vanadium dioxide films at terahertz range. Appl Surf Sci. 2015;331:92–97.
[19] Kiri P, Warwick MEA, Ridley I, et al. Fluorine doped vanadium dioxide thin films for smart windows. Thin Solid Films. 2011;520(4):1363–1366.
[20] Wan J, Ren Q, Wu N, et al. Density functional theory study of M-doped (M= B, C, N, Mg, Al) VO_2 nanoparticles for thermochromic energy-saving foils. J Alloy Compd. 2016;662:621–627.
[21] Quesada-Cabrera R, Powell MJ, Marchand P, et al. Scalable production of thermochromic Nb-Doped VO_2 nanomaterials using continuous hydrothermal flow synthesis. J Nanosci Nanotechno. 2016;16(9):10104–10111.
[22] Wang N, Shun NTC, Duchamp M, et al. Effect of lanthanum doping on modulating the thermochromic properties of VO_2 thin films. RSC Adv. 2016;6(54):48455–48461.
[23] Lv W, Huang D, Chen Y, et al. Synthesis and characterization of Mo-W co-doped VO_2 (R) nano-powders by the microwave-assisted hydrothermal method. Ceram Int. 2014;40(8):12661–12668.
[24] Abdellaoui I, Merad G, Maaza M, et al. Electronic and optical properties of Mg-, F-doped and Mg\F-codoped M1-VO_2 via hybrid density functional calculations. J Alloy Compd. 2016;658:569–575.
[25] Burkhardt W, Christmann T, Meyer BK, et al. W-and F-doped VO_2 films studied by photoelectron spectrometry. Thin Solid Films. 1999;345(2):229–235.
[26] Liang Z, Zhao L, Meng W, et al. Tungsten-doped vanadium dioxide thin films as smart windows with self-cleaning and energy-saving functions. J Alloy Compd. 2017;694:124–131.
[27] Zhang D, Yang K, Li Y, et al. Employing TiO_2 buffer layer to improve VO_2 film phase transition performance and infrared solar energy modulation ability. J Alloy Compd. 2016;684:719–725.
[28] Fan LL, Chen S, Luo ZL, et al. Strain dynamics of ultrathin VO_2 film grown on TiO_2 (001) and the associated phase transition modulation. Nano letters. 2014;14(7):4036–4043.
[29] Xiao H, Li Y, Yuan W, et al. Microstructures and thermochromic characteristics of VO_2/AZO composite films. Infrared Phys Techn. 2016;76:580–586.
[30] Gao YF, Wang SB, Luo HJ, et al. Enhanced chemical stability of VO_2 nanoparticles by the formation of SiO_2/VO_2 core/shell structures and the application to transparent and flexible VO_2-based composite foils with excellent thermochromic properties for solar heat control. Energ Environ Sci. 2012;5(3):6104–6110.

[31] Li Y, Ji S, Gao Y, et al. Core-shell VO_2@TiO_2 nanorods that combine thermochromic and photocatalytic properties for application as energy-saving smart coatings. Sci Rep-uk. 2013;3:1370.
[32] Xu G, Jin P, Tazawa M, et al. Optimization of antireflection coating for VO_2-based energy efficient window. Sol Energ Mat Sol C. 2004;83(1):29–37.
[33] Yu JH, Nam SH, Lee JW, et al. Enhanced visible transmittance of thermochromic VO_2 thin films by SiO_2 passivation layer and their optical characterization. Mater. 2016;9(7):556.
[34] Liu C, Wang N, Long Y. Multifunctional overcoats on vanadium dioxide thermochromic thin films with enhanced luminous transmission and solar modulation, hydrophobicity and anti-oxidation. Appl Surf Sci. 2013;283:222–226.
[35] Powell MJ, Quesada-Cabrera R, Taylor A, et al. Intelligent multifunctional VO_2/SiO_2/TiO_2 coatings for self-cleaning, energy-saving window panels. Chem Mater. 2016;28(5):1369–1376.
[36] Liu M, Su B, Kaneti YV, et al. Dual-phase transformation: spontaneous self-template surface-patterning strategy for ultra-transparent VO_2 solar modulating coatings. ACS Nano. 2016;11(1):407–415.
[37] Qian X, Wang N, Li Y, et al. Bioinspired multifunctional vanadium dioxide: improved thermochromism and hydrophobicity. Langmuir. 2014;30(35):10766–10771.
[38] Lu Q, Liu C, Wang N, et al. Periodic micro-patterned VO_2 thermochromic films by mesh printing. J Mater Chem C. 2016;4(36):8385–8391.
[39] Genzer J, Efimenko K. Recent developments in superhydrophobic surfaces and their relevance to marine fouling: a review. Biofouling. 2006;22(5):339–360.
[40] Zhu H, Guo Z, Liu W. Adhesion behaviors on superhydrophobic surfaces[J]. Chem Commun. 2014;50(30):3900–3913.
[41] Quéré D. Non-sticking drops. Rep Prog Phys. 2005;68(11):2495.
[42] Wang B, Zhang Y, Shi L, et al. Advances in the theory of superhydrophobic surfaces. J Mater Chem A. 2012;22(38):20112–20127.
[43] Manoudis PN, Tsakalof A, Karapanagiotis I, et al. Fabrication of super-hydrophobic surfaces for enhanced stone protection. Surf Coat Tech. 2009;203(10):1322–1328.
[44] Holzwarth U, Gibson N. The Scherrer equation versus the 'Debye-Scherrer equation'. Nat Nanotechnol. 2011 6(9):534–534.
[45] Pan M, Zhong H, Wang S, et al. Properties of VO_2 thin film prepared with precursor $VO(acac)_2$. J Cryst Growth. 2004;265(1):121–126.
[46] Xu G, Jin P, Tazawa M, et al. Tailoring of luminous transmittance upon switching for thermochromic VO_2 films by thickness control. Jpn J Appl Phys. 2004;43(1R):186.
[47] Li SY, Niklasson GA, Granqvist CG. Thermochromic fenestration with VO_2-based materials: three challenges and how they can be met. Thin Solid Films. 2012;520(10):3823–3828.
[48] Chen S, Luo CS, Dai L, et al. The visible transmittance and solar modulation ability of VO_2 flexible foils simultaneously improved by Ti doping: an optimization and first principle study. Phys Chem Chem Phys. 2013;15(40):17537–17543.
[49] Chen S, Ma H, Dai J, et al. Nanostructured vanadium dioxide thin films with low phase transition temperature. Appl Phys Lett. 2007;90(10):101117.
[50] Zhang S, Chou JY, Lauhon LJ. Direct correlation of structural domain formation with the metal insulator transition in a VO_2 nanobeam. Nano Let. 2009;9(12):4527–4532.
[51] Trarieux H. Effect of substitution on the vanadium dioxide phase transition. Influence changements phase prop. Phys Corps Solids. 1970;101:I14.
[52] Tang C, Georgopoulos P, Fine ME, et al. Local atomic and electronic arrangements in $W_xV_{1-x}O_2$. Phys Rev B. 1985;31(2):1000.
[53] Bowman RM, Gregg JM. VO_2 thin films: growth and the effect of applied strain on their resistance. J Mater Sci-Mater El. 1998;9(3):187–191.
[54] Kim GS, Hyun SH. Synthesis and characterization of silica aerogel films for inter-metal dielectrics via ambient drying. Thin Solid Films. 2004;460(1):190–200.
[55] Budunoglu H, Yildirim A, Guler MO, et al. Highly transparent, flexible, and thermally stable superhydrophobic ORMOSIL aerogel thin films. ACS Appl Mater Inter. 2011;3(2):539–545.
[56] Nishino T, Meguro M, Nakamae K, et al. The lowest surface free energy based on–CF_3 alignment. Langmuir. 1999;15(13):4321–4323.
[57] Miwa M, Nakajima A, Fujishima A, et al. Effects of the surface roughness on sliding angles of water droplets on superhydrophobic surfaces. Langmuir. 2000;16(13):5754–5760.
[58] Yabu H, Shimomura M. Single-step fabrication of transparent superhydrophobic porous polymer films. Chem Mater. 2005;17(21):5231–5234.
[59] Wang R, Hashimoto K, Fujishima A, et al. Watanabe, photogeneration of highly amphiphilic TiO_2 surfaces. Adv Mater. 1998;10(2):135–138.
[60] Feng X, Zhai J, Jiang L. The fabrication and switchable superhydrophobicity of TiO_2 nanorod films. Angew Chem Int Edit. 2005;44(32):5115–5118.